

Information-Preserving Contrastive Learning for Self-Supervised Representations

Tianhong Li^{*} Lijie Fan^{*} Yuan Yuan Hao He Yonglong Tian Dina Katabi
MIT CSAIL

Abstract

Contrastive learning is very effective at learning useful representations without supervision. Yet contrastive learning has its limitations. It may learn a shortcut that is irrelevant to the downstream task, and discard relevant information. Past work has addressed this limitation via custom data augmentations that eliminate the shortcut. This solution however does not work for data modalities that are not interpretable by humans, e.g., radio signals. For such modalities, it is hard for a human to guess which shortcuts may exist in the signal, or how they can be eliminated. Even for interpretable data, sometimes eliminating the shortcut may be undesirable. The shortcut may be irrelevant to one downstream task but important to another. In this case, it is desirable to learn a representation that captures both the shortcut information and the information relevant to the other downstream task. This paper presents information-preserving contrastive learning (IPCL), a new framework for unsupervised representation learning that preserves relevant information even in the presence of shortcuts. We empirically show that the representations learned by IPCL outperforms contrastive learning in supporting different modalities and multiple diverse downstream tasks.

1. Introduction

The area of unsupervised or self-supervised representation learning is growing rapidly (He et al., 2020; Doersch et al., 2015; Ye et al., 2019; Hjelm et al., 2018; Grill et al., 2020; Bachman et al., 2019; Zhuang et al., 2019; Misra & Maaten, 2020; Han et al., 2020). It refers to learning data representations that capture potential labels of interest, and doing so without human supervision. Contrastive learning is increasingly considered as a standard and highly competitive method for unsupervised representation learning. Features learned with this method have been shown to generalize

well to downstream tasks, and in some cases surpass the performance of supervised models (Oord et al., 2018; Caron et al., 2020; Tschannen et al., 2019; Chen et al., 2020a;b;c).

Contrastive learning learns representations by contrasting positive samples against negative samples. During training, a data sample is chosen as an anchor (e.g., an image); positive samples are chosen as different augmented versions of the anchor (e.g., randomly cropping and color distorting the image), whereas negative samples come from other samples in the dataset.

Despite its effectiveness, contrastive learning is vulnerable to shortcuts – i.e., if simple features are contrastive enough to separate positive samples from negative samples, contrastive learning might learn such simple (or simpler) features though they may be irrelevant to the tasks of interest, and ignore other more relevant features. For example, the authors of (Chen et al., 2020a) show that color distribution can be a shortcut to distinguish patches cropped from the same image, from patches from different images; yet such feature is not very useful for object classification. Past work manually designs data augmentations to break such shortcuts, so that the network may learn the relevant information (He et al., 2020; Chen et al., 2020a;b;c).

However, it is not always possible to address shortcuts via data augmentation. First, machine learning tasks are expanding to new modalities, many of which are not directly interpretable by humans such as radio signals (Zhao et al., 2018a;b; 2019; Li et al., 2019; Fan et al., 2020a;b), or acceleration data (Hsu et al., 2019; 2017; Fan et al., 2020a). Consider for example the task of through-wall pose estimation (Zhao et al., 2018a). This task leverages that radio signals traverse walls and occlusions and reflect off the human body; it designs neural network models that analyze the radio frequency (RF) signals and infer the human pose, even when people are behind a wall. Such task would benefit significantly from unsupervised representation learning given the limited amount of labeled RF signals, and the difficulties of labeling such modality which is not interpretable by human workers (Zhao et al., 2018a;b; 2019; Li et al., 2019). However, like RGB data, RF data can have shortcuts that make contrastive learning ineffective (see the results section

^{*}Equal contribution. Correspondence to: Lijie Fan <lijiefan@mit.edu>, Tianhong Li <tianhong@mit.edu>.

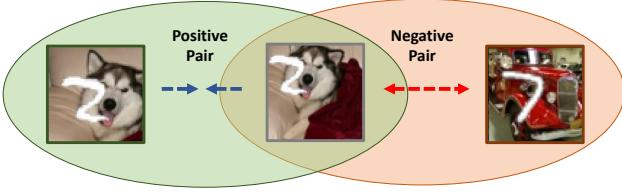


Figure 1. Shortcut Example. The input has two types of information: digit and background object, but existing contrastive learning methods generate a representation that focuses on the background object and ignores the digit.

for empirical validation). But unlike RGB data, it is hard for humans to guess what the shortcuts may be, or how to alter the RF signal to create data augmentations that eliminate the shortcuts, while preserving useful information.

Second, eliminating shortcut features is not always desirable, even for RGB-based tasks. Sometimes the shortcut features are irrelevant to one downstream task but important to another task. For example, the authors of (Tian et al., 2020) highlight the scenario in Figure 1, where each image shows a digit (from MNIST) on a randomly chosen background object (from STL-10). They show that features related to the background object can create a shortcut that prevents contrastive learning from learning features related to the digit. However, eliminating features about the background object is not desirable since ideally one would like a representation that works for both downstream tasks: digit classification, and background object classification.

To address the above problems, we propose a new framework that we call information-preserving contrastive learning (IPCL). The key idea underlying IPCL is to learn representations using contrastive and reconstructive learning simultaneously. We use the term reconstructive learning to refer to tasks that force the representation to reconstruct the input, such as inpainting, colorization, or autoencoding. Such tasks counter the effect of shortcuts because they force the learned features to both abstract and retain the information in the input. Once combined with reconstructive learning, contrastive learning ensures that all useful features (not just the shortcut features) are closely mapped in the embedding space for positive samples, and stay distant for negative samples. Thus, reconstructive learning maximizes the useful information in the representation, whereas contrastive learning orders the information in the embedding space to make it easy for a simple classifier to slice the embedding space to satisfy a desired task.

We evaluate IPCL and compare it with state-of-the-art contrastive learning baselines such as SimCLR (Chen et al., 2020a), MoCo (He et al., 2020), and Contrastive Predictive Coding (CPC) (Hénaff et al., 2019). We summarize our findings for RF and RGB data as follows:

(a) *Results on RF Data:* We evaluate IPCL on three real-world RF-based sensing tasks: 3D pose estimation, human

action recognition, and person re-identification. The results show that IPCL outperforms all contrastive learning baselines on all tasks. In comparison to the best performing contrastive learning baseline, the IPCL representation improves performance by 30.6 mm, 81.4 mAP, and 24.5 mAP on the tasks of pose estimation, action recognition, and person re-id respectively. Interestingly, the representations learned by the contrastive learning baselines perform worse than random features on pose estimation and action recognition. This shows that contrastive learning converged on a shortcut, and discarded key information necessary for these two tasks.

(b) *Results on RGB Data:* Since RF signals are hard to interpret, we apply IPCL to RGB data to gain more insight into its working. We evaluate IPCL on the Colorful-MNIST, a synthetic dataset proposed in (Tian et al., 2020) and illustrated in Figure 1. In comparison to the contrastive learning baselines, the IPCL representation has 72% lower error on digit classification and comparable performance on background classification. This shows that IPCL is better at generating representations that can support multiple downstream tasks. Even more, we show that increasing the size of the digit (by 10 to 15 pixels) causes the contrastive learning shortcut to move from background to digit, though the semantic information in each image did not change. In all cases, IPCL learns a representation that performs well on both digit and background classifications, whereas the representation learned by contrastive learning is good only for at most one of the two tasks.

To summarize, our paper has the following contributions:

- We introduce IPCL, the first self-supervised learning framework that integrates contrastive and reconstructive learning to automatically avoid shortcuts and provide a representation that supports multiple different downstream tasks. We note that while both contrastive and reconstructive learning existed prior to our work, no past work has discovered their complementary role or proposed to combine them the way we do.
- We empirically show the negative impact shortcuts have on contrastive learning, and how a shortcut can move from one task to another, though the input semantics did not change. We also show that IPCL addresses these issues.
- Finally, we are the first to study unsupervised representation learning from radio signals, demonstrating the possibility of boosting the performance of RF-based human sensing tasks by leveraging unlabeled RF signals.

2. Related Work

(a) **Unsupervised Contrastive Representation Learning:** Early work on unsupervised representation learning has focused on designing pretext tasks and training the network to predict the pseudo labels for those tasks. Such tasks

include solving Jigsaw Puzzles (Noroozi & Favaro, 2016), restoring a missing patch in the input (Pathak et al., 2016), or predicting image rotation (Gidaris et al., 2018). However, pretext tasks have to be handcrafted, and the generality of their representations is typically limited (Chen et al., 2020a).

Hence, researchers have recently focused on contrastive learning, which emerged as a competitive and systematic method for learning effective representations without human supervision. The learned features generalize well to downstream tasks, outperform representations learned through pretext tasks, and even surpass the performance of supervised models on some tasks (Chen et al., 2020a;b;c; He et al., 2020). Multiple successful contrastive learning frameworks have been proposed, which typically differ in the way they sample negative pairs. To name a few, SimCLR (Chen et al., 2020a) uses a large batch-size, and samples negative pairs within each batch. The momentum-contrastive approach (MoCo) (He et al., 2020) leverages a moving-average encoder and a queue to generate negative samples on-the-fly during training. Contrastive-Multiview-Coding (Tian et al., 2019) maintains a memory-bank to store features, and generates negative samples from this memory bank.

Past work has also reported some limitations of contrastive learning. The authors of (Chen et al., 2020a) showed that color distribution can be a shortcut, and proposed to break this shortcut through color-distortion data augmentation. Further, the authors of (Tian et al., 2020) noted that when the data includes multiple types of semantics, one type may produce a shortcut that prevents contrastive learning from learning effective features of other semantics (as is the case in Figure 1, where the background object information can be a shortcut that prevents learning information related to the digit in the image). They proposed a solution that learns contrastive views suitable for the desired downstream task. While they share our goal of supporting different downstream tasks, their method requires supervision since they learn their contrastive views from labeled data. In contrast, our representation learning is completely unsupervised.

Another related work is contrastive-predictive-coding (CPC) (Oord et al., 2018; Hénaff et al., 2019). CPC has some similarity with IPCL in that it has a predictive task that aims to reconstruct missing information. However, CPC aims to reconstruct the features of a future frame, while IPCL reconstructs the raw input data. As a result, the representation learned by CPC is not forced to contain necessary information to reconstruct the input, making it susceptible to shortcuts, just like other contrastive learning methods.

(b) Learning from Radio Signals: There is a growing literature that leverages radio signals to learn pose estimation, action recognition, captioning, and re-identifications through walls and occlusions (Zhao et al., 2018a;b; 2019; Wang et al., 2019; Li et al., 2019; Chetty et al., 2017; Zhang

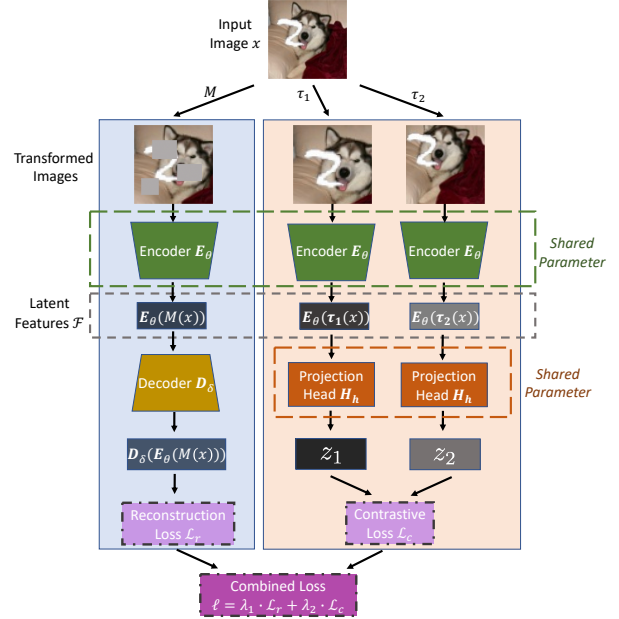


Figure 2. Illustration of the IPCL framework for RGB data. The framework has two branches: 1) a reconstructive branch, illustrated in the blue box, which ensures that the representation has enough information to restore the missing patches in the input, and 2) a contrastive branch, illustrated in the orange box, which ensures that the representation keeps positive samples close to each other and away from negative samples.

et al., 2018; Fan et al., 2020b;a; Hsu et al., 2019; Vasishth et al., 2018). Past work however relies on supervised learning from annotated data. Given the difficulty of annotating RF datasets with ground truth labels for pose or actions, past work is limited to relatively small datasets, which hampers its performance. Our work allows these models to leverage large amounts of unannotated RF signals to improve the performance of their downstream tasks.

3. IPCL

Information-preserving contrastive learning (IPCL) is a framework for self-supervised representation learning. It aims to learn representations that are robust to shortcuts, and capable of supporting multiple diverse downstream tasks. IPCL aims to provide these properties without knowing a priori the potential shortcuts or the downstream tasks.

To achieve its goals, IPCL uses reconstructive learning and contrastive learning simultaneously. By ensuring that the representation can reconstruct the input, IPCL avoids shortcuts and ensures that the representation has as much information as the input. By ensuring that the representation is contrastive, IPCL ensures that samples close to each other semantically are close to each other in the feature space.

Figure 2 shows the IPCL framework for RGB data. An IPCL model has two branches: a contrastive learning branch, and

a reconstructive learning branch. The goal of IPCL is to train a good encoder network that generates a representation that simultaneously minimizes the contrastive loss and the reconstructive loss.

(a) Reconstructive Branch: To choose a proper reconstructive task, we need to consider two aspects: its ability to summarize and abstract the input, and its applicability to different modalities. In fact, the vast majority of self-supervised learning tasks, such as Auto-encoder, Colorization, Inpainting and Jigsaw Puzzle, are reconstructive since they all aim to reconstruct the input. However, those tasks do not have the same ability to both retain and abstract the information at the input. For example, inpainting is a stronger reconstructive task than colorization or autoencoding in terms of its ability to both retain and abstract information. Thus, although any of these reconstructive tasks would help in strengthening contrastive learning against shortcuts, inpainting is likely to provide more gains.

Another issue to consider is the applicability of the chosen task to various modalities. For example, colorization is applicable only to RGB, and Jigsaw does not naturally translate to RF signals.¹ In contrast, a task like inpainting is easier to translate across modalities by cropping random windows of the signal.

Given the above two considerations, we adopt inpainting as the default reconstructive task. In Sec. 5.3, we compare these various reconstructive tasks and show that while all reconstructive tasks improve performance, inpainting delivers higher gains and works across modalities.

Figure 2 shows how IPCL uses the inpainting task for RGB data, where given an input image x , we first randomly mask several patches to get the masked input $M(x)$. Then the masked input is passed through an encoder network E with parameter θ , and a decoder network D , with parameter δ , to obtain the reconstruction result $D_\delta(E_\theta(M(x)))$. The reconstruction loss \mathcal{L}_r is defined as the reconstruction error between the original input x and the reconstructed one $D_\delta(E_\theta(M(x)))$:

$$\mathcal{L}_r = \|D_\delta(E_\theta(M(x))) - x\|_2.$$

(b) Contrastive Branch: The contrastive branch is illustrated in the orange box in Figure 2. For each image, we first generate a pair of positive samples by using two random augmentations τ_1 and τ_2 , then we forward the two augmented inputs separately into the encoder E parameterized by θ and a multi-layer nonlinear projection head H parameterized by h to get the latent representations z_1 and z_2 for these two positive samples. We use the commonly used InfoNCE loss (Chen et al., 2020a) as the contrastive

loss \mathcal{L}_c . Namely, for a batch of N different input images $x_i, i = 1, \dots, N$,

$$\mathcal{L}_c = - \sum_{i=1}^N \log \sum_{k=1}^{2N} \frac{\exp(\text{sim}(z_{2i}, z_{2i+1})/t)}{\mathbb{1}_{k \neq 2i} \exp(\text{sim}(z_{2i}, z_k)/t)},$$

where $\text{sim}(u, v) = u^T v / (\|u\|_2 \|v\|_2)$ denotes the dot product between the normalized u and v (i.e., cosine similarity), $t \in \mathbb{R}^+$ is a scalar temperature parameter, and z_{2i}, z_{2i+1} are the encoded features of positive pairs generated from x_i , i.e., $z_{2i} = H_h(E_\theta(\tau_1(x_i)))$ and $z_{2i+1} = H_h(E_\theta(\tau_2(x_i)))$.

(c) Training Procedure: We have empirically found that it is better to train the model in two phases. In the first phase, only the reconstructive branch is trained. In the second phase, both branches are trained together. In this latter case, the overall training loss is the combination of the reconstruction loss and the contrastive loss, i.e.:

$$\mathcal{L} = \lambda_1 \cdot \mathcal{L}_r + \lambda_2 \cdot \mathcal{L}_c$$

4. Adapting IPCL to RF Signals

Next, we adapt IPCL to learn useful representations from unlabeled RF signals. Since RF signals are not interpretable by a human, past work generates annotation by deploying a camera system and synchronizing it with the RF device, which is labor-intensive and hard to scale. If we can learn useful representation from unlabeled RF signals, we reduce overhead and improve the accuracy of downstream tasks.

4.1. Overview of Human Sensing using RF Signals

We would like to learn self-supervised representation useful for the following tasks:

- (a) RF-Based 3D Pose Estimation (Zhao et al., 2018a;b), which uses radio signals to infer the 3D locations of 14 keypoints on the human body that denote the head, neck, shoulders, arms, wrists, hip, knees, and feet.
- (b) RF-Based action recognition (Li et al., 2019), which analyses radio signals to infer human actions and interactions in the presence of occlusions and in poor lighting.
- (b) RF-Based Re-Id (Fan et al., 2020b), which recognizes a person-of-interest across different places and times by analyzing the radio signals that bounce off their bodies.

In all of these tasks, the input is a time sequence of RF frames. Each RF frame is a pair of 2D heatmaps: one horizontal heatmap and one vertical heatmap, as illustrated in Figure 3. The horizontal heatmap is a projection of the radio signals on a plane parallel to the ground, and the vertical heatmap is a projection of the radio signals on a plane perpendicular to the ground. There are typically 30 pairs of heatmaps per second.

The models used in RF-based human sensing tasks have the general structure in Figure 4. The model first uses a spatio-temporal convolutional feature network to extract features

¹There is a complex dependence between the signals in the vertical heatmap and horizontal heatmap, which would be broken if one simply rearrange these voxels.

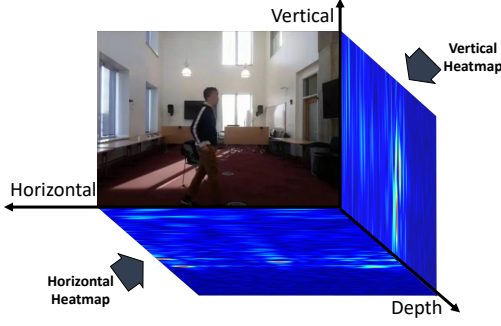


Figure 3. Illustration of RF signals as a pair of horizontal and vertical heatmaps, and an RGB image recorded at the same time. Red color refers to high signal power and blue refers to low power.

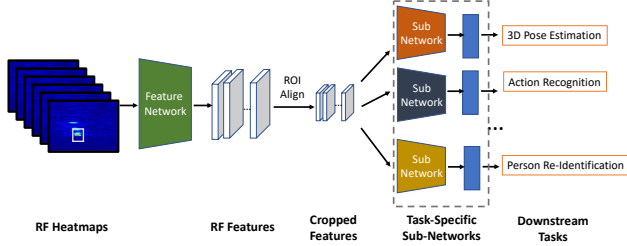


Figure 4. RF-based human sensing framework. The RF heatmaps are first fed into a Feature Network to extract spatio-temporal features, and ROI Align with the given bounding box is used to crop out the regions with humans. Each downstream task has a unique sub-network to extract task-specific features and predictions.

from the input RF frames. It then crops out a bounding box around the person in the feature map. Finally, the cropped features are fed into a task-specific sub-network to generate frame-level features for downstream tasks. The high-level structure is the same for all tasks, but different tasks have different sub-networks specifically designed for that task.

4.2. IPCL for RF Signals

To apply IPCL to RF signals, we use the network in Figure 5. The reconstructive task predicts missing RF frames. Specifically, for each RF sequence consisting of 100 RF frames, we randomly mask out 25 frames within this sequence and fill them with zeros. The reconstructive task reconstructs the original RF sequence using the learned feature. For contrastive learning, as shown in Figure 5, the anchor and positive sample share the same input RF frames with different random jitter of the bounding boxes. Frames that are within 0.3 seconds of the anchor frame serve as positive samples. Negative samples of an anchor are all samples in the batch except for itself and its positive sample.

During the unsupervised learning phase, a spatio-temporal RF feature extraction network, the same as the feature network in Figure 4, is used to encode the input RF frames. Then an ROI Align is applied on top of the extracted features to crop out the region around the person, where the bounding boxes are generated using the WiTrack localiza-

tion algorithm (Adib et al., 2014). For contrastive learning, a non-linear projection head consisting of 3 convolutional residual blocks and 2 fully-connected layers is added on top of the cropped feature maps to project the features and apply the contrastive loss l_P between features from positive and negative samples. For the reconstruction task, a decoder is added to reconstruct the masked RF frames, and a per-pixel reconstruction loss l_C is added between the reconstructed RF and the ground truth RF frames. We then combine these two losses together as $\lambda_1 \cdot l_P + \lambda_2 \cdot l_C$.

5. Evaluation

5.1. Experiments with RGB Data

Dataset. To better understand the impact of shortcuts on contrastive learning and IPCL, we experiment with Colorful-MNIST, a synthetic dataset proposed by the authors of (Tian et al., 2020). It is constructed by assigning each digit from MNIST a background object image selected randomly from the STL-10 dataset. Hence, each image in the Colorful-MNIST dataset has two types of semantic information that correspond to the digit class and the background object class. Figure 1 shows some typical samples from this dataset.

Reconstructive Branch. We use the inpainting task for the reconstructive branch. For each input image after augmentation with a size of 64 by 64 pixels, we randomly mask out 3 to 5 rectangle patches at random locations in the image and fill them with the average pixel value of the dataset. The size of each square is chosen by setting its side randomly between 10 and 16 pixels.

Contrastive Branch. For the contrastive branch in IPCL, as in (Chen et al., 2020a), we apply random cropping and random color jittering on an image twice to generate positive pairs. The negative pairs are sampled within a batch.

Network Structure. We use a 6-layer ConvNet for the encoder E . The encoder weights for the predictive and contrastive branches are shared. The decoder D is a 6-layer deconvolutional network symmetric to E . The projection head H for contrastive learning is a 2-layer non-linear head which embeds the feature into a 64-dim normalized space.

Baselines. We use state-of-the-art contrastive learning methods as baselines, including SimCLR (Chen et al., 2020a), MoCo (He et al., 2020) and CPC (Hénaff et al., 2019). We also include Inpainting (Pathak et al., 2016) as another baseline. The same network structure is used for all baselines and for IPCL’s contrastive branch. The hyper-parameters for each baseline are fine-tuned to achieve its best performance. Other implementation details are provided in Appendix.

5.1.1. RGB RESULTS

We evaluate the performances of IPCL and baselines under both fixed feature extractor setting and fine-tuning setting.

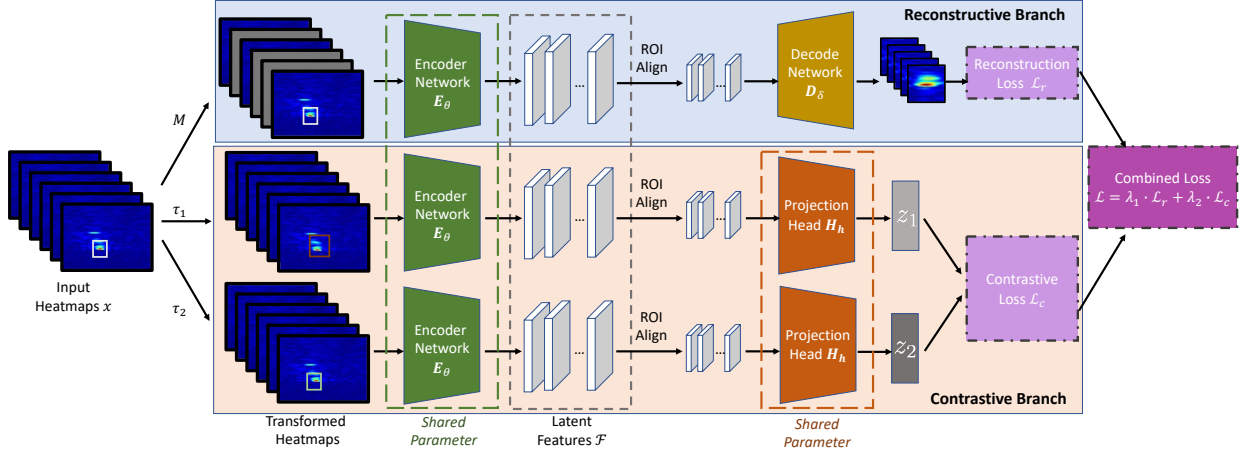


Figure 5. IPCL on RF signals. For the reconstructive branch, we randomly mask some RF frames. For the contrastive branch, different transformation τ_1 and τ_2 to the bounding box are adopted to generate positive samples. Both branches share the same feature extraction network (Green Box), and then use ROI Align with the given bounding box to crop out regions containing humans. The reconstructive branch has a decoder to reconstruct inputs, while the contrastive branch has a non-linear projection head to generate normalized features. The combination of reconstruction loss and contrastive loss is used to train the model.

Method		digit cls. error rate (%)	bkgd cls. error rate (%)
fixed feature extractor	SimCLR	85.1	51.5
	MoCo	84.3	53.7
	CPC	84.2	64.8
	Inpainting	15.3	65.0
	IPCL (ours)	11.7	54.0
fine- tuning	SimCLR	7.6	45.1
	MoCo	7.3	45.2
	CPC	7.7	45.3
	Inpainting	7.1	45.5
	IPCL (ours)	6.7	45.3
Supervised on digit		3.9	88.6
Supervised on bkgd		87.1	43.3
Supervised on digit bkgd		7.0	45.5

Table 1. We study the representation quality learned from Colorful-MNIST using different unsupervised methods. We evaluate the learned representation on the downstream tasks of digit classification and background object classification.

Two linear classifiers are added on top of the pre-trained feature extractor for two downstream tasks: digit classification and background object classification. For the fixed feature extractor setting, only the two linear classifiers are trained; for the fine-tuning setting, the feature extractor is trained together with the classifiers.

Table 1 reports the error rate for each method. It reveals the following findings:

- None of the contrastive learning baselines can learn features that capture information relevant to digit classification. In fact, their error rate on digit classification (84% to 85%) is similar to the error rate of a supervised method where the feature extractor was trained only on background object classification with no information about

digits ($\sim 88\%$). The contrastive learning baselines perform reasonably well on background object classification with an error rate $\sim 10\%$ higher than a supervised method trained on that task. This indicates that the background object features played the role of a shortcut for contrastive learning, i.e., those features were sufficient to contrast positive and negative samples, and hence there was no need for contrastive learning to learn digit-related features.

- IPCL on the other hand learned a representation that is useful for both digit and background object classifications. Its error rate on background object classification is comparable to the baselines, but its error rate on digit classification is $\sim 70\%$ lower than the contrastive baselines. Further, because of its contrastive branch, IPCL can learn better features for both digit and background classification than inpainting. (The Appendix provides a tSNE visualization of the learned features.)

5.1.2. WHAT IS A SHORTCUT?

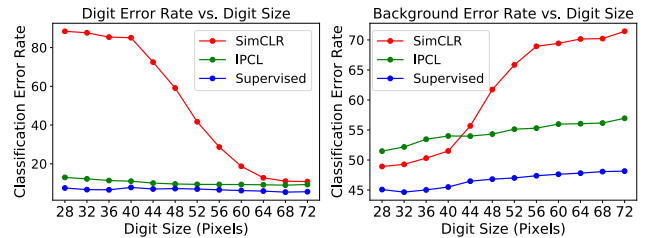


Figure 6. Contrastive learning shortcuts change even when the input semantics does not change. The figure plots the classification error rate vs. different digit sizes for the Colorful-MNIST dataset. The left figure shows the digit classification error while the right one shows the background classification error.

It might seem that certain semantics are shortcuts, e.g., background texture is a shortcut that prevents learning digit-related features. Here we show that shortcuts are not neces-

sarily related to a particular type of semantic information. Since Colorful-MNIST is a synthetic dataset, we can adjust the size of the MNIST digit added on the background image. In Figure. 6, we study the performance change of SimCLR and IPCL when adding MNIST digits with different sizes onto a background of STL-10 images. The figure shows that as the digit size increases, the shortcut that SimCLR learns shifts from learning only the background object information to learning only the foreground digit information. This shows that it is very hard to determine which information contrastive learning will focus on, and which it will ignore: simply changing the digit size will change the shortcut, though the input semantics did not change. On the other hand, IPCL exhibit robust performance with different digit sizes. The results in Figure. 6 demonstrate the complexity of reasoning about shortcuts even in RGB images, and how IPCL overcomes this complexity.

5.2. Experiments with RF Datasets

We evaluate IPCL on three through-wall RF sensing tasks: pose estimation, action recognition, and re-identification.

Datasets. We pre-train IPCL on two real-world RF datasets: RF-MMD (Li et al., 2019) and RRD (Fan et al., 2020a). RF-MMD is an RF-based pose estimation and action recognition dataset consisting of 25 hours of RF data with 30 volunteers performing 35 actions in 10 different indoor environments. RRD is an RF-based person re-identification dataset. It contains 863 RF sequences from 100 different identities at 5 different locations on a university campus, and 6305 RF sequences from 38 different identities in 19 homes.

Evaluation Metrics. We use the performance metrics used by past work for each task. Specifically, for 3D pose estimation, we use the average l_2 distance between 14 predicted keypoints and their ground-truth locations as the evaluation metric. For action recognition, we use mean average precision (mAP) at different intersection-over-union (IoU) thresholds θ to evaluate the accuracy of the model in detecting and classifying an action event. For person re-identification, we separate the dataset into query set and gallery set. The query samples and gallery samples are then encoded to feature vectors. We calculate the cosine distance between the features of each query sample and each gallery sample, and rank the distance to get the top-N closest gallery samples for each query sample. Based on the ranking results, we compute the mean average precision (mAP) and the cumulative matching characteristic (CMC) at rank-1 and rank-5.

Evaluation Settings. We evaluate the performance of IPCL and baselines under both fixed feature extractor setting and fine-tuning setting. In the fixed feature extractor setting, we use the pre-trained RF feature extractor as initialization of the RF feature extractor for each downstream task, but this feature network is frozen during downstream task

training, i.e., only those task-specific sub-networks (4) are trained. In the fine-tuning setting, we use the self-supervised representation as an initialization, which gets fine-tuned during training on each task –i.e., we use the pre-trained RF feature extractor to initialize the feature extractor for each downstream task, and fine-tune the whole model on the downstream task. We use the RF-MMD dataset for downstream tasks of pose estimation and action recognition, and the RRD dataset for person re-identification.

Baselines. Since there is no prior work that applies existing contrastive learning methods on RF data, we implement SimCLR (Chen et al., 2020a), MoCo (He et al., 2020), CPC (Hénaff et al., 2019) and Inpainting (Pathak et al., 2016) on RF data by ourselves as baselines. The SimCLR implementation is similar to the contrastive branch of IPCL, and the inpainting implementation is similar to the reconstructive branch of IPCL. For MoCo, we use the same data augmentation operations as SimCLR, except the positive feature pairs are generated by two feature networks, a normal one and a momentum one. The loss is the same as the one used in (He et al., 2020). For CPC, we follow the design in (Hénaff et al., 2019). Specifically, we add a GRU RNN after the RF feature extractor. The output of the GRU at every frame is then used as the context to predict the features in 1.5s in the future using the contrastive loss. We also train a supervised baseline from scratch for the fine-tuning setting, and a randomly initialized RF feature extractor serves as a baseline for the fixed feature extractor setting.

5.2.1. RF RESULTS

We evaluate the RF feature extractor learned by IPCL on multiple downstream RF-based tasks. The results are shown in Table 2 and 3. As shown in the results, pre-training the feature network using IPCL performs the best for all tasks in both settings. Under the fixed feature extractor setting, IPCL is the only method that is comparable to supervised training. Under the fine-tuning setting, compared to its supervised counterparts, IPCL has 8.6% relative improvement in 3D pose estimation error, 3.7% relative improvement in action recognition mAP at $\theta = 0.1$, 2.2% relative improvement in person ReID mAP on RRD-Campus, and 3.6% relative improvement on RRD-Home.

The tables also show that the feature network pre-trained using contrastive learning alone can generate worse results than random initialization. For example, in Table 2, training a pose sub-network on top of an RF feature extractor with random weights can get 60.1 pose error, while training a pose sub-network on top of the feature extractor pre-trained using SimCLR, MoCo and CPC can only get 80.5, 77.2 and 78.7 mm pose error, respectively. This is likely due to that contrastive learning learns shortcut semantics irrelevant to human sensing, and thus is harmful to human-related downstream tasks. Note that although CPC also uses a predictive

	3D Pose Estimation	Action Recognition		Person Re-ID (Campus)			Person Re-ID (Home)		
Methods	Pose Err.↓ (mm)	mAP↑		mAP↑	CMC-1↑	CMC-5↑	mAP↑	CMC-1↑	CMC-5↑
		$\theta = 0.1$	$\theta = 0.5$						
Random init	60.1	70.5	53.3	28.1	43.8	68.8	30.1	54.2	74.6
SimCLR	80.5	4.2	0	29.8	44.1	67.5	31.2	55.1	73.8
MoCo	77.2	5.1	0.18	29.1	44.7	65.3	30.5	54.5	74.0
CPC	78.7	3.6	0	30.0	42.7	69.5	30.7	54.0	75.3
Inpainting	51.1	72.3	65.5	49.8	73.1	90.5	38.5	64.2	84.7
IPCL	46.6	86.5	83.1	54.5	78.7	93.0	43.3	72.4	87.6
Supervised	38.4	90.1	87.8	59.5	82.1	95.5	46.4	74.6	89.5

Table 2. Evaluation of different models on different RF datasets and tasks under fixed feature extractor setting, where the RF feature encoder is initialized with pre-trained model using unsupervised learning methods, and the weights are frozen during downstream training. ↓ indicates the smaller the value, the better the performance; ↑ indicates the larger the value, the better the performance.

	3D Pose Estimation	Action Recognition		Person Re-ID (Campus)			Person Re-ID (Home)		
Methods	Pose Err.↓ (mm)	mAP↑		mAP↑	CMC-1↑	CMC-5↑	mAP↑	CMC-1↑	CMC-5↑
		$\theta = 0.1$	$\theta = 0.5$						
Random init	38.4	90.1	87.8	59.5	82.1	95.5	46.4	74.6	89.5
SimCLR	38.8	89.8	87.4	59.0	81.7	94.1	45.9	73.8	88.5
MoCo	38.3	89.7	87.2	59.3	82.0	94.5	46.4	74.3	89.7
CPC	38.6	89.9	87.5	59.4	81.5	94.0	46.0	74.5	89.1
Inpainting	36.2	91.7	88.7	60.1	83.3	95.5	47.5	75.3	90.3
IPCL	35.1	92.5	89.6	60.8	84.2	96.0	48.1	76.1	91.0

Table 3. Evaluation of different models on different RF datasets and tasks under fine-tuning setting, where the RF feature encoder is initialized with pre-trained model using unsupervised learning methods, and then fine-tuned during downstream training. ↓ indicates the smaller the value, the better the performance; ↑ indicates the larger the value, the better the performance.

task, its prediction is performed on the feature space and thus cannot guarantee the information in the input to be preserved in the learned representation. Using the reconstruction task alone without the contrastive loss can generate better results than training from scratch, but the performance is worse than that of IPCL. This is because inpainting alone tends to learn low-level features too close to the pixels in the RF heatmaps, and fail to learn abstract features about the human body. In contrast, IPCL is able to utilize the combination of contrastive and reconstructive learning to learn abstract and information-preserving features that are useful for downstream tasks. The above results further show that the feature extractor learned by IPCL can extract representations that contain multiple types of semantics related to various downstream tasks.

5.3. Ablation Study on Reconstructive Tasks

	RF-MMD	Colorful-MNIST	
Recon. Tasks	Pose Err.	digit cls. error rate	bkgd cls. error rate
No Recon.	80.5	85.1	51.5
Colorization	N/A	39.9	54.5
Jigsaw Puzzle	N/A	22.9	59.3
Autoencoder	51.1	34.4	57.1
Inpainting	46.6	11.7	54.0

Table 4. Evaluation of different reconstructive tasks.

In IPCL, we choose the inpainting task for the reconstructive branch. However, other reconstructive tasks can be potentially used for the reconstructive branch. In this section, we evaluate the performance of IPCL with different reconstructive tasks including inpainting, auto-encoder, colorization (Zhang et al., 2016), and Jigsaw Puzzle (Noroozi & Favaro, 2016). Table 4 shows IPCL’s performance using different reconstructive task on RF-based 3D pose estimation (RF-MMD) and Colorful-MNIST under the fixed feature extractor setting. As shown in the table, all reconstructive tasks significantly reduce errors in comparison to using contrastive learning without any reconstruction task. The table also shows that inpainting compares favorably to other tasks and works across modalities. Hence, we use inpainting as the default reconstructive task in IPCL.

6. Conclusion

In this paper, we introduce information-preserving contrastive learning, a novel framework to keep unsupervised contrastive learning effective and preserve useful information in the presence of shortcuts. We apply our framework to RGB data to show its ability to solve the problem of shortcuts. We further adapt our framework to RF data to demonstrate the possibility of boosting performance of RF-based human sensing tasks with unsupervised learning. Extensive experiments on both RGB and RF data demonstrate the effectiveness of our proposed framework.

References

- Adib, F., Kabelac, Z., Katabi, D., and Miller, R. C. 3d tracking via body radio reflections. In *11th {USENIX} Symposium on Networked Systems Design and Implementation ({NSDI} 14)*, pp. 317–329, 2014.
- Andriluka, M., Pishchulin, L., Gehler, P., and Schiele, B. 2d human pose estimation: New benchmark and state of the art analysis. In *Proceedings of the IEEE Conference on computer Vision and Pattern Recognition*, pp. 3686–3693, 2014.
- Bachman, P., Hjelm, R. D., and Buchwalter, W. Learning representations by maximizing mutual information across views. *arXiv preprint arXiv:1906.00910*, 2019.
- Caron, M., Misra, I., Mairal, J., Goyal, P., Bojanowski, P., and Joulin, A. Unsupervised learning of visual features by contrasting cluster assignments. *arXiv preprint arXiv:2006.09882*, 2020.
- Chen, T., Kornblith, S., Norouzi, M., and Hinton, G. A simple framework for contrastive learning of visual representations. *arXiv preprint arXiv:2002.05709*, 2020a.
- Chen, T., Kornblith, S., Swersky, K., Norouzi, M., and Hinton, G. E. Big self-supervised models are strong semi-supervised learners. *Advances in Neural Information Processing Systems*, 33, 2020b.
- Chen, X., Fan, H., Girshick, R., and He, K. Improved baselines with momentum contrastive learning. *arXiv preprint arXiv:2003.04297*, 2020c.
- Chetty, K., Chen, Q., Ritchie, M., and Woodbridge, K. A low-cost through-the-wall fmcw radar for stand-off operation and activity detection. In *Radar Sensor Technology XXI*, volume 10188, pp. 1018808. International Society for Optics and Photonics, 2017.
- Doersch, C., Gupta, A., and Efros, A. A. Unsupervised visual representation learning by context prediction. In *Proceedings of the IEEE international conference on computer vision*, pp. 1422–1430, 2015.
- Fan, L., Li, T., Fang, R., Hristov, R., Yuan, Y., and Katabi, D. Learning longterm representations for person re-identification using radio signals. In *Proceedings of the IEEE/CVF Conference on Computer Vision and Pattern Recognition*, pp. 10699–10709, 2020a.
- Fan, L., Li, T., Yuan, Y., and Katabi, D. In-home daily-life captioning using radio signals. *arXiv preprint arXiv:2008.10966*, 2020b.
- Gidaris, S., Singh, P., and Komodakis, N. Unsupervised representation learning by predicting image rotations. *arXiv preprint arXiv:1803.07728*, 2018.
- Grill, J.-B., Strub, F., Altché, F., Tallec, C., Richemond, P. H., Buchatskaya, E., Doersch, C., Pires, B. A., Guo, Z. D., Azar, M. G., et al. Bootstrap your own latent: A new approach to self-supervised learning. *arXiv preprint arXiv:2006.07733*, 2020.
- Han, T., Xie, W., and Zisserman, A. Memory-augmented dense predictive coding for video representation learning. *arXiv preprint arXiv:2008.01065*, 2020.
- He, K., Fan, H., Wu, Y., Xie, S., and Girshick, R. Momentum contrast for unsupervised visual representation learning. In *Proceedings of the IEEE/CVF Conference on Computer Vision and Pattern Recognition*, pp. 9729–9738, 2020.
- Hénaff, O. J., Srinivas, A., De Fauw, J., Razavi, A., Doersch, C., Eslami, S., and Oord, A. v. d. Data-efficient image recognition with contrastive predictive coding. *arXiv preprint arXiv:1905.09272*, 2019.
- Hjelm, R. D., Fedorov, A., Lavoie-Marchildon, S., Grewal, K., Bachman, P., Trischler, A., and Bengio, Y. Learning deep representations by mutual information estimation and maximization. *arXiv preprint arXiv:1808.06670*, 2018.
- Hsu, C.-Y., Ahuja, A., Yue, S., Hristov, R., Kabelac, Z., and Katabi, D. Zero-effort in-home sleep and insomnia monitoring using radio signals. *Proceedings of the ACM on Interactive, Mobile, Wearable and Ubiquitous Technologies*, 1(3):1–18, 2017.
- Hsu, C.-Y., Hristov, R., Lee, G.-H., Zhao, M., and Katabi, D. Enabling identification and behavioral sensing in homes using radio reflections. In *Proceedings of the 2019 CHI Conference on Human Factors in Computing Systems*, pp. 1–13, 2019.
- Kärkkäinen, K. and Joo, J. Fairface: Face attribute dataset for balanced race, gender, and age. *arXiv preprint arXiv:1908.04913*, 2019.
- Li, T., Fan, L., Zhao, M., Liu, Y., and Katabi, D. Making the invisible visible: Action recognition through walls and occlusions. In *Proceedings of the IEEE International Conference on Computer Vision*, pp. 872–881, 2019.
- Misra, I. and Maaten, L. v. d. Self-supervised learning of pretext-invariant representations. In *Proceedings of the IEEE/CVF Conference on Computer Vision and Pattern Recognition*, pp. 6707–6717, 2020.
- Noroozi, M. and Favaro, P. Unsupervised learning of visual representations by solving jigsaw puzzles. In *European Conference on Computer Vision*, pp. 69–84. Springer, 2016.
- Oord, A. v. d., Li, Y., and Vinyals, O. Representation learning with contrastive predictive coding. *arXiv preprint arXiv:1807.03748*, 2018.
- Pathak, D., Krahenbuhl, P., Donahue, J., Darrell, T., and Efros, A. A. Context encoders: Feature learning by inpainting. In *Proceedings of the IEEE conference on computer vision and pattern recognition*, pp. 2536–2544, 2016.
- Tian, Y., Krishnan, D., and Isola, P. Contrastive multiview coding. *arXiv preprint arXiv:1906.05849*, 2019.
- Tian, Y., Sun, C., Poole, B., Krishnan, D., Schmid, C., and Isola, P. What makes for good views for contrastive learning. *arXiv preprint arXiv:2005.10243*, 2020.
- Tschannen, M., Djolonga, J., Rubenstein, P. K., Gelly, S., and Lucic, M. On mutual information maximization for representation learning. *arXiv preprint arXiv:1907.13625*, 2019.
- Vasht, D., Jain, A., Hsu, C.-Y., Kabelac, Z., and Katabi, D. Duet: Estimating user position and identity in smart homes using intermittent and incomplete rf-data. *Proceedings of the ACM on Interactive, Mobile, Wearable and Ubiquitous Technologies*, 2(2):1–21, 2018.

- Wang, F., Zhou, S., Panev, S., Han, J., and Huang, D. Person-in-wifi: Fine-grained person perception using wifi. In *Proceedings of the IEEE/CVF International Conference on Computer Vision*, pp. 5452–5461, 2019.
- Xiao, B., Wu, H., and Wei, Y. Simple baselines for human pose estimation and tracking. In *Proceedings of the European conference on computer vision (ECCV)*, pp. 466–481, 2018.
- Ye, M., Zhang, X., Yuen, P. C., and Chang, S.-F. Unsupervised embedding learning via invariant and spreading instance feature. In *Proceedings of the IEEE Conference on computer vision and pattern recognition*, pp. 6210–6219, 2019.
- Zhang, R., Isola, P., and Efros, A. A. Colorful image colorization. In *European conference on computer vision*, pp. 649–666. Springer, 2016.
- Zhang, Z., Tian, Z., and Zhou, M. Latern: Dynamic continuous hand gesture recognition using fmcw radar sensor. *IEEE Sensors Journal*, 18(8):3278–3289, 2018.
- Zhao, M., Li, T., Abu Alsheikh, M., Tian, Y., Zhao, H., Torralba, A., and Katabi, D. Through-wall human pose estimation using radio signals. In *Proceedings of the IEEE Conference on Computer Vision and Pattern Recognition*, pp. 7356–7365, 2018a.
- Zhao, M., Tian, Y., Zhao, H., Alsheikh, M. A., Li, T., Hristov, R., Kabelac, Z., Katabi, D., and Torralba, A. Rf-based 3d skeletons. In *Proceedings of the 2018 Conference of the ACM Special Interest Group on Data Communication*, pp. 267–281, 2018b.
- Zhao, M., Liu, Y., Raghu, A., Li, T., Zhao, H., Torralba, A., and Katabi, D. Through-wall human mesh recovery using radio signals. In *Proceedings of the IEEE International Conference on Computer Vision*, pp. 10113–10122, 2019.
- Zhuang, C., Zhai, A. L., and Yamins, D. Local aggregation for unsupervised learning of visual embeddings. In *Proceedings of the IEEE/CVF International Conference on Computer Vision*, pp. 6002–6012, 2019.

Appendix A: Implementation Details

In this section, we provide the implementation details of the models used in our experiments. All experiments are performed on 8 NVIDIA Titan X Pascal GPUs. We note that the parameters for each baseline are chosen to optimize for its best performance.

Digit & Background Object Classification: For the baseline approaches (SimCLR, MoCo and CPC), we use the SGD optimizer with 0.1 learning rate, $1e-4$ weight decay, and 0.9 momentum to train the model for 200 epochs. We note that we tried both Adam and SGD, and picked SGD since it performed better, which is consistent with prior work (Chen et al., 2020a; He et al., 2020). The learning rate is scaled with a factor of 0.1 at epoch 150 and 175. The batch size is set to 512. The temperature for contrastive loss is set to 0.1. For IPCL, the network is trained for 200 epochs with the Adam optimizer. We also tried both SGD and Adam and found that Adam is better for training IPCL. This may be because the Adam optimizer is better for optimizing the reconstructive loss as reported in (Pathak et al., 2016). The learning rate is set to $1e-3$. The first 50 epochs are warm-up epochs, where we only train the network with the reconstruction loss \mathcal{L}_r . We set $\lambda_1 = 40$ and $\lambda = 1$.

RF Experiments: For the baseline contrastive approach, we train the network for 50 epochs, using the SGD optimizer with 0.01 learning rate, $1e-5$ weight decay and 0.9 momentum. For IPCL, we train the network using the Adam optimizer with $1e-3$ learning rate and $1e-5$ weight decay. The network is trained for 50 epochs with the first 10 epochs as warm-up epochs trained with only the reconstruction loss. We set $\lambda_1 = 100$ and $\lambda = 1$.

Appendix B: Experiments on Real-World RGB Datasets

In the main paper, we illustrate the impact of shortcuts on contrastive learning and IPCL using a synthetic Colorful-MNIST dataset, and further demonstrate IPCL’s effectiveness on solving this problem using multiple real-world RF datasets and tasks. In this section, we further show that shortcuts can also cause severe problem even on common RGB datasets and tasks, such as face attributes classification and human pose estimation, and that IPCL can also outperform traditional contrastive learning under these settings.

B.1: Experiments on Face Dataset

In this section, we evaluate IPCL on FairFace (Kärkkäinen & Joo, 2019), a real world human face attribute dataset, where each image contains multiple semantics including gender, age, and ethnicity, as shown in Figure 7.

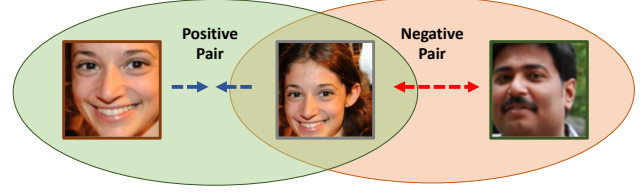


Figure 7. Illustration of FairFace dataset. The positive pairs are from random cropping and random color jittering on an image twice. The negative pairs are sampled within batch.

B.1.1 EXPERIMENT SETUP

Reconstructive Setting. We use the strategy in (Pathak et al., 2016) to mask out 3 to 5 rectangles at random locations in the image. The size of each square is chosen by setting its side randomly between 7 and 12 pixels. We fill the masked rectangles with the mean pixel value.

Contrastive Setting. For contrastive learning, we follow the strategy in (Chen et al., 2020a) to sample positive and negative pairs. We apply random cropping and random color jittering on an image twice to generate positive pairs. The negative pairs are sampled within batch.

Network Structure. We use a standard ResNet-18 for the encoder network. The decoder network is a symmetric de-convolutional network. The projection head for contrastive learning is a 2-layer non-linear head which embed the feature into a 128-dimensional unit sphere.

Evaluation Metric. We evaluate the learned representations on three downstream tasks: age, gender and ethnicity classification. For the training of the downstream tasks, we freeze the encoder and train a linear layer for each task to classify the features. For the supervised baselines, supervised (a), (g) and (e) are trained on the single task of age, gender and ethnicity, respectively, while supervised (all) is jointly trained on all the three tasks.

Baselines. We compare IPCL with SimCLR, MoCo and CPC. The same network structure is used for all baselines and for IPCL’s contrastive branch. The hyper-parameters for each baseline are fine-tuned to achieve its best performance.

Implementation Details. For the SimCLR baseline, we train the network for 1000 epochs using the SGD optimizer with 0.1 learning rate, $1e-4$ weight decay and 0.9 momentum. The learning rate is scaled with a factor of 0.2 at epoch 450, 600 and 750. The batch size is set to 512. The temperature for contrastive loss is set to 0.1. For MoCo, the data augmentation is the same as SimCLR, and the number of negative samples is set to $K = 16384$. For CPC, following (Oord et al., 2018), we extract 7×7 grid with 50% overlap from the original image, extract features from grids, and apply contrastive loss to the features within five rows. For IPCL, the network is trained for 500 epochs, using the Adam

optimizer with $1e-3$ learning rate. The first 100 epochs are warm-up epochs, where we only train the network with the reconstruction loss \mathcal{L}_r .

B.1.2 RESULTS

Table 5 compares the performance of state-of-the-art contrastive learning and IPCL on the FairFace dataset. As shown by the supervised baselines, the three tasks share some common features since network trained on one of the task can also be used to classify other tasks with reasonable accuracy. However, each task also has its unique features since there are still big performance gaps between network trained on the specific task of interest and networks trained on the other two tasks. The table also shows that IPCL’s performances on age and gender are significantly better than all baselines. Although achieving the best performance among the three baselines, SimCLR’s performance on age and gender are similar to that of supervised learning on ethnicity label alone ($\sim 56\%$ and $\sim 21\%$ error rate, respectively). This is possibly because the shortcut for contrastive learning is more related to the ethnicity than to age and gender. IPCL improves over SimCLR’s performance on age and gender classification by 5.7% and 8.6% respectively, while keeping comparable performance to SimCLR on ethnicity classification (38.8% vs. 37.7%). This further demonstrates IPCL’s ability to preserve useful information that could be ignored by contrastive learning.

Method	age cls. error rate (%)	gender cls. error rate (%)	ethnicity cls. error rate (%)
SimCLR	55.7	21.4	37.7
MoCo	56.1	21.9	38.3
CPC	56.5	23.8	39.0
IPCL (ours)	50.0	12.8	38.8
Supervised (a)	44.5	21.3	54.9
Supervised (g)	56.7	7.5	54.6
Supervised (e)	57.9	23.2	28.6
Supervised (all)	45.2	8.1	29.2

Table 5. We study the representation quality learnt using different methods. We evaluate the learned representation on downstream tasks of age, gender and ethnicity classification.

B.2: Experiments on Human Pose Estimation Dataset

We also evaluate IPCL on MPII (Andriluka et al., 2014) human pose dataset. This dataset contains images of everyday human activities, and is one of the most common dataset for the task of human pose estimation.

B.2.1 EXPERIMENT SETUP

The major implementation details for IPCL on MPII is similar to the one for Face Dataset, as described in Appendix

B.1.1. Here we only list the settings that are different.

Reconstructive Setting. We mask out 6 to 8 rectangles at random locations in the image. The size of each square is chosen by setting its side randomly between 30 and 50 pixels.

Network Structure. We use the network structure similar to the one in (Xiao et al., 2018). We use a ResNet-50 for the encoder network. Three deconvolutional layers with kernel size 4 and one convolutional layer with kernel size 1 is added on top of the encoded feature to transfer the feature into 13 heatmaps corresponding to 13 keypoints. For the contrastive branch, a 2-layer non-linear projection head is added on top of the encoded feature and embed the feature into a 128-dimensional unit sphere. For the reconstructive branch, a decoder network similar to the pose estimation deconvolution network (only the number of output channels is changed to 3) is used to reconstruct the original image.

Evaluation Metric. We evaluate the learned representations under the single pose estimation setting (Andriluka et al., 2014). Each person is cropped using the approximate location and scale provided by the dataset. Similar to prior works, we report the PCKh (Percentage of Correct Keypoints that uses the matching threshold as 50% of the head segment length) value of each keypoint and an overall weighted averaged PCKh over all keypoints (head, shoulder, elbow, wrist, hip, knee, ankle). We evaluate the representations under two different settings: fixed feature encoder setting and fine-tuning setting. In the fixed feature encoder setting, the ResNet encoder is fixed and only the 4-layer decoder network is trained; In the fine-tuning setting, the encoder is initialized with the pre-trained model and fine-tuned during training.

B.2.2 RESULTS

We list the performance for IPCL and various baseline approaches in Table 9. Under both settings, IPCL outperforms SimCLR by a large margin: 3.7 PCKh under fixed feature encoder setting and 0.7 PCKh under fine-tuning setting. This is possibly because SimCLR can fall into shortcuts that are irrelevant to human poses such as the texture of the clothes, while the Inpainting task alone possibly focuses only on features related to detailed pixels but failed to learn high-level features. On the other hand, IPCL is able to learn abstract and information-preserving features and thus achieve good performance.

Appendix C: Ablation Study

We perform extensive ablation studies to better understand the good practices for applying IPCL to RGB and RF data. The RGB ablation studies are performed on Colorful-MNIST dataset with the downstream task of digit and back-

Method		Head [↑]	Shoulder [↑]	Elbow [↑]	Wrist [↑]	Hip [↑]	Knee [↑]	Ankle [↑]	PCKh [↑]
fixed feature extractor	Random init	30.3	31.4	20.2	13.8	25.8	18.1	17.5	23.9
	SimCLR	79.0	75.2	57.3	45.8	62.4	51.9	47.7	61.4
	Inpainting	83.4	75.2	53.6	44.4	56.4	44.3	45.7	59.0
	IPCL (ours)	85.7	78.8	61.7	51.3	64.4	55.6	49.2	65.1
fine- tuning	Random init	96.3	95.1	87.9	82.2	87.8	82.7	77.8	87.7
	SimCLR	96.2	94.7	87.3	81.2	87.5	81.0	77.2	87.1
	Inpainting	96.3	95.2	87.9	82.1	87.8	82.5	77.6	87.7
	IPCL (ours)	96.3	94.9	88.1	82.3	87.9	82.8	77.8	87.8

Table 6. We study the representation quality learned from MPII using different unsupervised methods. We evaluate the learned representation on the downstream task of human pose estimation. [↑] indicates the larger the value, the better the performance. Note that the pose estimation here is in 2D image and the RF-based pose estimation in the main paper is in 3D, so the evaluation metrics are also different.

ground object classification, and the RF ablation studies are performed on RF-MMD (Li et al., 2019) dataset with the downstream task of pose estimation, where we report the average error across all keypoints.

C.1 RGB Data

Cropping Strategy: We first compare the performance of IPCL with different cropping/masking strategies (recall that cropping is used in the reconstruction task in IPCL). We compare 3 different strategies: center region (25x25 patch in the center of the input image), random region (25x25 patch at a random position in the input image), and random patches (3 to 5 rectangle patches at random locations in the image. The size of each rectangle is chosen by setting its side randomly between 10 and 16 pixels.). As shown in the results below, the random-patches strategy performs the best.

Cropping Strategy	Digit cls. err. (%)	Bkgd cls. err. (%)
Center Region	25.5	58.1
Random Region	20.1	56.2
Random Patches	11.7	54.0

Table 7. Classification error rate with different image cropping strategies.

Size of Cropped Patches: Next, We study the influence of the sidesize of each masked patch. Note that when the size is equal to 0, no patches are cropped, and the reconstruction branch becomes a normal auto-encoder. In all of these experiments, we follow the strategy of randomly selecting 3 to 5 rectangle patches of fixed sidesize. As shown in Figure 8, the best performance on digit classification is to apply patches with sidesize of 10 pixels and the best performance on background object classification is to apply patches with sidesize of 16 pixels. Therefore, we finally choose the size of each rectangle by setting its side randomly between 10 and 16 pixels to optimize for both classification task.

Warm-up Training: As explained in the paper, IPCL has a warm-up training phase in which it uses only the reconstruction loss. To show the effectiveness of the proposed

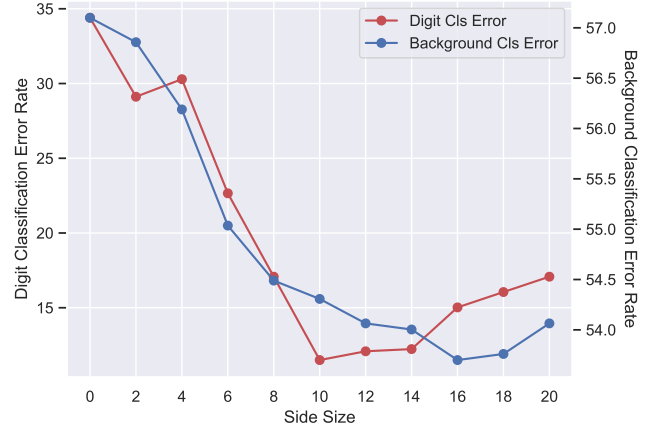


Figure 8. Classification error rate with different sizes of masked patches.

warm-up training strategy, we compare the results of warm-up training with the results of directly using the combined loss \mathcal{L} (i.e., combining the reconstruction loss and the contrastive loss) from the beginning:

Warm-up Training	Digit cls. err. (%)	Bkgd cls. err. (%)
Yes	11.7	54.0
No	75.1	52.8

Table 8. Classification error rate with and without warm-up training.

As shown in Table 8, without the warm-up training phase, IPCL largely degenerates to become similar to the contrastive learning baselines and cannot learn good features related to digit classification. This indicates that without the warm-up phase, the contrastive loss can dominate the network causing it to only learn the shortcut of background object classification at the beginning, and that the network cannot later jump out of the local minimum associated with the shortcut. On the other hand, with warm-up training, the network first learns a coarse representation useful for both digit and background classification; then the contrastive loss

helps the network learn more fine-grained representations.

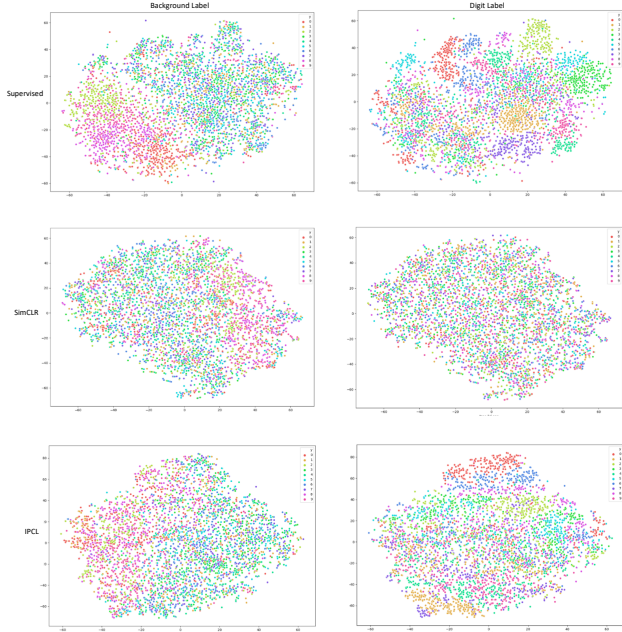


Figure 9. Feature visualization of supervised learning, SimCLR and IPCL using tSNE on Colorful-Moving-MNIST.

Feature Visualization: We further visualize the features learned by SimCLR, IPCL and supervised learning in Figure 9 using tSNE. The left column is colored using background object labels, and the right column is colored using digit labels. Features generated by both supervised learning and IPCL forms clusters under both coloring methods, while SimCLR only shows clustering when colored using background object label. This further shows that contrastive learning will focus on certain shortcut and ignore features relevant to other tasks, while features learned by IPCL can preserve both information and achieve good performance on both downstream tasks.

C.2: RF data

We also perform ablation studies on applying IPCL to real-world RF datasets. All ablation studies are performed on RF-MMD (Li et al., 2019) dataset with the downstream task of pose estimation, where we report the average error across all keypoints.

Masking Strategy: When applied to RF signals, IPCL’s reconstruction task is performed by masking some frames in a short window RF signals, and reconstructing them from the remaining frames. We compare the performance of IPCL with different masking strategies. The input RF signal is a 100-frames RF sequence. We compare 3 different masking strategies: center segment (25 frames in the center of the input), random segments (five 5-frames segments at random positions of input), and random (each frame is masked with 0.25 probability). As shown in the results below, the random

segments masking strategy performs the best.

Mask Strategy	Skeleton Error (cm)
Center Segment	3.58
Random Segments	3.51
Random	3.53

Table 9. Skeleton error (the lower the better) with different masking strategies.

Size of Masked Segment: Next, We study the influence of the size of each masked segment. Note that when the mask size equals to 0, no frame is masked, and the reconstruction branch becomes a normal auto-encoder. In all of these experiments, we mask 5 segments and follow the strategy of randomly locating the masked segments in the input. As shown in Table 10, the best performance is for masking 5 consecutive frames, i.e., a segment of size 5.

Masking Size	0	1	3	5	10
Skeleton Err. (cm)	3.68	3.60	3.52	3.51	3.60

Table 10. Skeleton error with different sizes of masked segments.

Warm-up Training: To show the effectiveness of the proposed warm-up training strategy on RF signals, we compare the results of warm-up training with the results of directly using the combined loss \mathcal{L} (i.e., combining the reconstruction loss and the contrastive loss) from the beginning:

Warm-up Training	Skeleton Error (cm)
Yes	3.51
No	3.83

Table 11. Skeleton error (the lower the better) with and without warm-up training.

As shown in Table 11, without the warm-up training, IPCL performs similar to just applying the contrastive loss without adding the reconstructive loss (3.88 cm skeleton error as reported in Table 3 of the paper). This indicates that without the warm-up phase, the contrastive loss can dominate the network causing it to learn the shortcut at the beginning, and that the network cannot later jump out of the local minimum associated with the shortcut. On the other hand, with warm-up training, the network first learns a coarse representation of the RF signals; then the contrastive loss helps the network learn more fine-grained representations.

Benefits of Unlabeled Data: To show the effectiveness of the proposed method in utilizing large unlabeled RF dataset, we simulate the scenario where only a handful of labeled RF data is available and a large amount of RF data is unlabeled data. Specifically, we randomly select 10% of the training set of RF-MMD to be RF-MMD-L to serves as the small

labeled dataset. We compare the performance of IPCL when it is pretrained on RF-MMD-L and RF-MMD and finetuned on RF-MMD-L.

Methods	Skeleton Error (cm)
Training from scratch (RF-MMD-L)	4.87
IPCL on RF-MMD-L+finetune	4.50
IPCL on RF-MMD+finetune	4.21

Table 12. Skeleton error (the lower the better) with different IPCL training dataset.

As shown in 12, IPCL can improve the performance of RF-based pose estimation without using any additional unlabeled data. This is because IPCL can learn a general representation of RF signals and thus provide better generalization ability. Indeed, IPCL improves the skeleton error by 0.29 cm by leveraging the unlabeled data. This demonstrates the potential of using IPCL to leverage large-scale unlabeled RF data to improve the performance of RF-based human sensing methods.